AIAA-2004-0437

42nd AIAA Aerospace Sciences Meeting and Exhibit
5-8 January 2004, Reno Hilton, Nevada, USA

Parallel, high-order overset grid implementation for supersonic flows

By

Kehinde Alabi[!]
Thaerocomp Technical Corp.
Stony Brook, NY 11790

Foluso Ladeinde[*]
Mechanical Engineering Department
SUNY Stony Brook
Stony Brook, NY 11794-2300

In this paper, a high-order, parallel overset grid solver is formulated for the solution of supersonic flows. The solver combines the Padé compact scheme with the weighted essentially non-oscillatory (WENO) scheme. The compact scheme provides high-order spatial differencing in smooth flows fields, while the WENO formulation is suited for flows containing discontinuities. The overset procedure for smooth flow fields uses high-order centered interpolation methods. For discontinuous fields, the selection of the stencil for interpolation follows the standard WENO procedure for spatial differencing. The developed procedure was validated using analytical test functions for both smooth and discontinuous fields. The interpolated values of the functions were compared with the known values of the function. The flux preservation property of the overset scheme was also verified. Applications including the flow past a circular cylinder and 3D sphere are presented for smooth flows. Supersonic flow over a cylinder at Mach number, Ma = 2.15 was also analyzed with the newly developed overset procedure. Results indicate superior performance of high-order interpolation compared to low order methods. In the presence of discontinuities, the shock-capturing high order interpolation procedure proposed in this paper performs better than procedures that use centered interpolation, particularly in the vicinity of discontinuities.

[*] Research Engineer, Ph.D.
[!] Associate Fellow, AIAA; Associate Professor

1. Introduction

High order finite difference procedures have been shown to be more accurate and require less grid points than low-order methods[1,2]. The procedures have been applied to problems utilizing direct numerical and large eddy simulations[3,4] and in aeroacoustics[5,6] and electromagnetics[7-9] calculations.

Geometric complexity has forced computational fluid dynamicists to use overset grids[10-13] in order to be competitive with procedures based on unstructured grid topologies. Using finite-difference procedure with overset grids, problems such as complete airplanes and reentry vehicles[14-16] have been solved. However, overset procedures have typically used low-order interpolation to exchange results in the common regions.[15,16] When used with low-order flow solvers, second-order interpolation procedures may be adequate for exchanging results across boundaries. With high-order flow solvers, the low-order overset interpolation procedures will reduce solution accuracy, particularly in the vicinity of the overset boundaries. Several authors have examined the use of high-order interpolation procedures at boundaries of overset domains.[17-20] In particular, Sherer and Scott[20] compared several high-order interpolation methods, including explicit Lagrange, implicit Lagrange, and B-spline methods using a high-order compact difference solver. Their results show improved solutions with high-order methods. The attractive features of the high-order explicit Lagrange interpolation method when compared with the other high-order methods were also discussed. The former is used as the interpolation procedure in the current work, although a limited number of tests were carried out using high-order finite-element type shape functions.

The interest in this paper is on flow fields with shock waves, or other discontinuous fields[21,22]. The discontinuity-capturing procedure used in the present work is based on the weighted essentially non-oscillatory (WENO) procedure.[23,24] Without discontinuities, interpolation procedures typically select a stencil such that an overlapped node is centrally positioned within a set of selected interpolation points or stencil.[20] In the presence of a shock wave, for example, such a procedure could dissipate the shock wave and/or result in Gibbs oscillation at the boundary. Therefore, one would expect problems when a shock wave extends across an overset domain. The main objective of the current work is to examine the results when shock waves are present and both the overset interpolation and base procedures are high order. We also wish to compare the performance of the basic interpolation methods to one that utilizes a shock-capturing procedure. We report on the development of a high-order overset procedure for a general-purpose, high-order solver. For discontinuous flow fields, the procedure selects high-order overset stencils with shock-capturing abilities similar to the stencils used in WENO. The solver allows solution with both the compact difference method (smooth fields) and the WENO procedure (discontinuous fields).

A description of the overset procedure is provided in Section 2 of this paper. The WENO scheme is described in section 3. Validation of the overset procedure is discussed for smooth and discontinuous fields, in section 4. Analytical functions are used for this purpose. The flux conservation properties of the development procedures are also discussed – section 4. The application of the procedure to the flow past a cylinder (smooth), sphere (smooth), and bow shock in supersonic low are presented in section 5. Concluding remarks are provided in section 6.

2. The Overset Procedure

The overset procedure presented in this paper is discussed under three subtopics:

- Identification of the overset nodes
- Identification of the donors for the overset nodes
- Interpolation and donation of solution values to the overset nodes

Details of this tasks are provided below.

2.1 Identification of overset nodes

Overset nodes are the nodes that lie at the boundary of an overlap region. The boundary of an overlap region may be the edge of a grid or an edge exposed following a hole-cutting process. For a high order solver, the boundary condition at the edge may require a buffer of several nodes to maintain high-order accuracy at the edge of the domain. In such a case, additional buffer nodes may also be treated as overset nodes. For instance for a fourth-order solver, at least two nodes at the boundary will require boundary conditions, and thus, will be overset nodes at an overlap boundary.

For a sixth order solver, for instance, figure 1 illustrates the selection of overset nodes at the boundary of a hole cut in a grid – labeled grid 1. The grid 1 overlaps a second grid, grid 2, which contains a solid boundary. There is a buffer of three overset nodes at the boundary of grid 1 since the solver requires a buffer of three nodes to maintain high order up to the boundary.

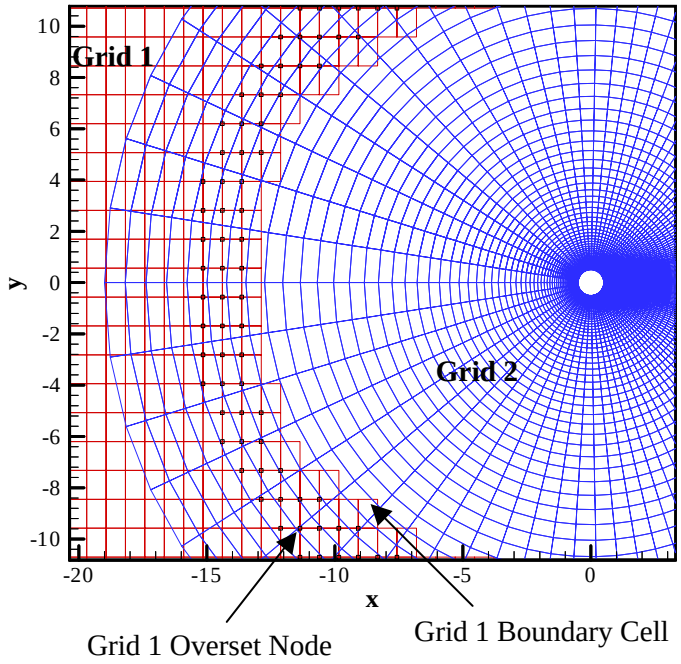

Figure 1. Overset nodes identified at the boundary of an overlapping grid

2.2 Identification of donors for overset nodes

Once the overset nodes are identified, they must be provided solution results via interpolation from another grid (overlapping the overset node). The boundary condition in an overset node is Dirichlett. The process of identifying donors involves a search within other grids to obtain a donor cell. Then, the offset of the overset node within the donor cell is calculated. To determine the offset, an inverse transformation procedure is used, as described below:

2.2.1 The Inverse Transformation Procedure

Given an overset (recipient) node located within a cell of a donor grid, shown in computational space in Figure 2, the value of the corresponding offset of the overset node within the donor cell can be obtained via an iterative scheme. To accomplish this purpose, a function relating the offset in computational space to physical space (f_1, f_2, f_3) is constructed.

A Taylor expansion of the function (f_1, f_2, f_3) relating (ξ, η, ζ) in computational space to (x, y, z) in physical space may be written as:

$$f_{i+1} = f_i + f_i' \Delta f_i + \ldots$$

Using Newton-Raphson formula we obtain

$$f_i' \Delta f_i = -f_i$$

where

$$\Delta f = \begin{bmatrix} \Delta f \\ \Delta f \\ \Delta f \end{bmatrix} = \begin{bmatrix} \frac{\partial f_1}{\partial \xi}\Delta\xi + \frac{\partial f_1}{\partial \eta}\Delta\eta + \frac{\partial f_1}{\partial \zeta}\Delta\zeta \\ \frac{\partial f_2}{\partial \xi}\Delta\xi + \frac{\partial f_2}{\partial \eta}\Delta\eta + \frac{\partial f_2}{\partial \zeta}\Delta\zeta \\ \frac{\partial f_3}{\partial \xi}\Delta\xi + \frac{\partial f_3}{\partial \eta}\Delta\eta + \frac{\partial f_3}{\partial \zeta}\Delta\zeta \end{bmatrix}$$

and

$$\Delta\xi = \xi_{i+1} - \xi_i$$
$$\Delta\eta = \eta_{i+1} - \eta_i$$
$$\Delta\zeta = \zeta_{i+1} - \zeta_i$$

Solving for ($\Delta\xi$, $\Delta\eta$, $\Delta\zeta$) via a matrix inversion , we obtain the following iterative procedure:

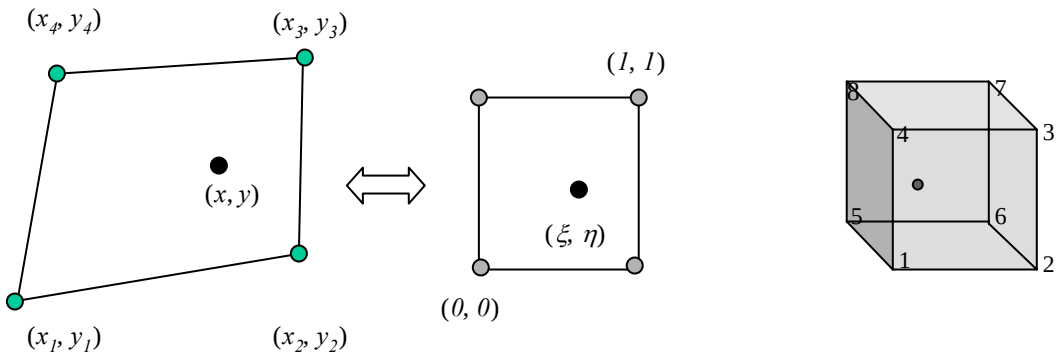

(a) 2D Physical Space (b) 2D Computational Space (c) 3D Computational Space

Figure 2. Overset node enclosed within a donor cell in computation space

$$\xi_{i+1} = \xi_i - J\left[\left(\frac{\partial f_2}{\partial \eta}\frac{\partial f_3}{\partial \zeta} - \frac{\partial f_2}{\partial \zeta}\frac{\partial f_3}{\partial \eta}\right)f_1 - \left(\frac{\partial f_1}{\partial \eta}\frac{\partial f_3}{\partial \zeta} - \frac{\partial f_1}{\partial \zeta}\frac{\partial f_3}{\partial \eta}\right)f_2 + \left(\frac{\partial f_1}{\partial \eta}\frac{\partial f_2}{\partial \zeta} - \frac{\partial f_1}{\partial \zeta}\frac{\partial f_2}{\partial \eta}\right)f_3\right]$$

$$\eta_{i+1} = \eta_i - J\left[\left(\frac{\partial f_1}{\partial \xi}\frac{\partial f_3}{\partial \zeta} - \frac{\partial f_1}{\partial \zeta}\frac{\partial f_3}{\partial \xi}\right)f_2 - \left(\frac{\partial f_2}{\partial \xi}\frac{\partial f_3}{\partial \zeta} - \frac{\partial f_2}{\partial \zeta}\frac{\partial f_3}{\partial \xi}\right)f_1 - \left(\frac{\partial f_1}{\partial \xi}\frac{\partial f_2}{\partial \zeta} - \frac{\partial f_1}{\partial \zeta}\frac{\partial f_2}{\partial \xi}\right)f_3\right]$$

$$\zeta_{i+1} = \zeta_i - J\left[\left(\frac{\partial f_2}{\partial \xi}\frac{\partial f_3}{\partial \eta} - \frac{\partial f_2}{\partial \eta}\frac{\partial f_3}{\partial \xi}\right)f_1 - \left(\frac{\partial f_1}{\partial \xi}\frac{\partial f_3}{\partial \eta} - \frac{\partial f_1}{\partial \eta}\frac{\partial f_3}{\partial \xi}\right)f_2 + \left(\frac{\partial f_1}{\partial \xi}\frac{\partial f_2}{\partial \eta} - \frac{\partial f_1}{\partial \eta}\frac{\partial f_2}{\partial \xi}\right)f_3\right]$$

where

$$J = \frac{1}{\frac{\partial f_1}{\partial \xi}\frac{\partial f_2}{\partial \eta}\frac{\partial f_3}{\partial \zeta} - \frac{\partial f_1}{\partial \xi}\frac{\partial f_3}{\partial \eta}\frac{\partial f_2}{\partial \zeta} - \frac{\partial f_1}{\partial \eta}\frac{\partial f_2}{\partial \xi}\frac{\partial f_3}{\partial \zeta} - \frac{\partial f_3}{\partial \xi}\frac{\partial f_2}{\partial \eta}\frac{\partial f_1}{\partial \zeta} + \frac{\partial f_2}{\partial \xi}\frac{\partial f_3}{\partial \eta}\frac{\partial f_1}{\partial \zeta} + \frac{\partial f_3}{\partial \xi}\frac{\partial f_1}{\partial \eta}\frac{\partial f_2}{\partial \zeta}}$$

The equations (f_1, f_2, f_3) in (ξ, η, ζ) may be chosen as some interpolation function such as explicit Lagrange interpolants or other interpolation function. In the current work, the form of the iterative equation chosen was the 64-node finite-element basis function, to maintain a high-order accuracy of the inverse transform:

$$f_1(\xi,\eta,\zeta) = \sum x_i N_i - x$$
$$f_2(\xi,\eta,\zeta) = \sum y_i N_i - y$$
$$f_3(\xi,\eta,\zeta) = \sum z_i N_i - z$$

and

$$N_i = N_i(\xi,\eta,\zeta)$$

where (x, y, z) is the physical coordinate whose (ξ, η, ζ) offset need to be determined within an enclosing donor cell.

Guess values for (ξ, η, ζ) are obtained from the metrices of the transformed domain as follows:

$$\xi = \xi_x \Delta x + \xi_y \Delta y + \xi_z \Delta z$$
$$\eta = \eta_x \Delta x + \eta_y \Delta y + \eta_z \Delta z$$
$$\zeta = \zeta_x \Delta x + \zeta_y \Delta y + \zeta_z \Delta z$$

Overset nodes for which a donor is not found are referred to as orphan nodes.

2.2.2 Projection of Cells at Solid Boundaries

In an overset formulation, projection of grid cells is sometimes necessary when two overset grids meet close to a curved solid boundary[25]. Such a situation is illustrated in figure 3 for a concave and convex solid boundary.

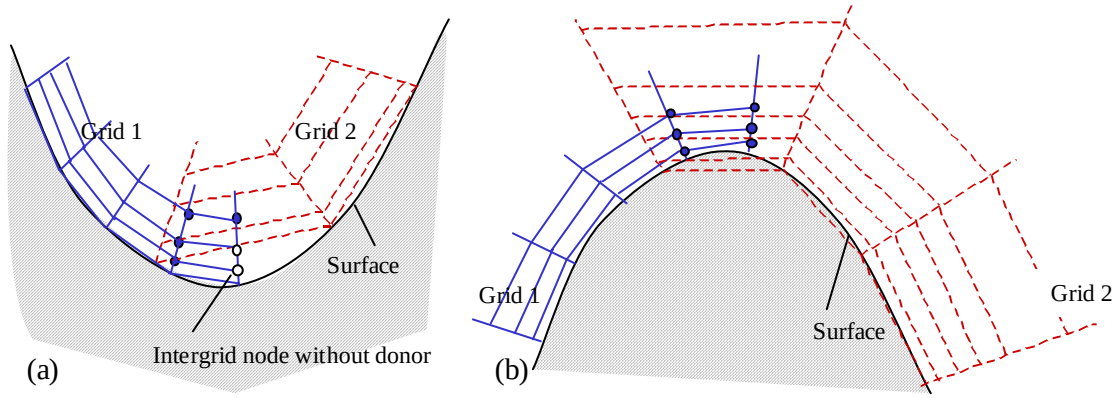

Figure 3. Illustration of the projection problem (a) concave surface, (b) convex surface

In this figure, Grid 1, overset within the domain of Grid 2, requires the flow results for its overset nodes. In the case of the concave surface, two of the overset nodes of Grid 1 appear to be orphans and can not receive interpolation results from any cell in Grid 2. Note that extrapolated results from Grid 2 will provide wrong results along the boundary of Grid 1.

In the case of the convex surface, the overset nodes of Grid 1 which are on the boundary cell will be receiving results from cells away from the boundary in Grid 2. This will produce abnormally high velocities close to the boundary of Grid 1.

To overcome this problem, the donating cells are projected as shown in figure 4.

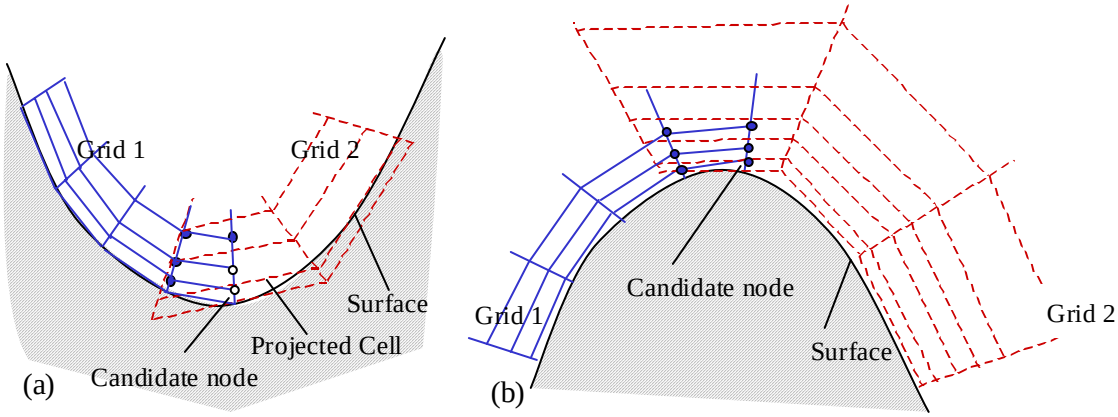

Figure 4. Illustration of the projection process (a) concave surface, (b) convex surface

Projection is done as part of the second phase of an overset problem (finding donors for overset nodes). The current procedure uses a local projection approach. The flow chart for this procedure is shown in figure 5.

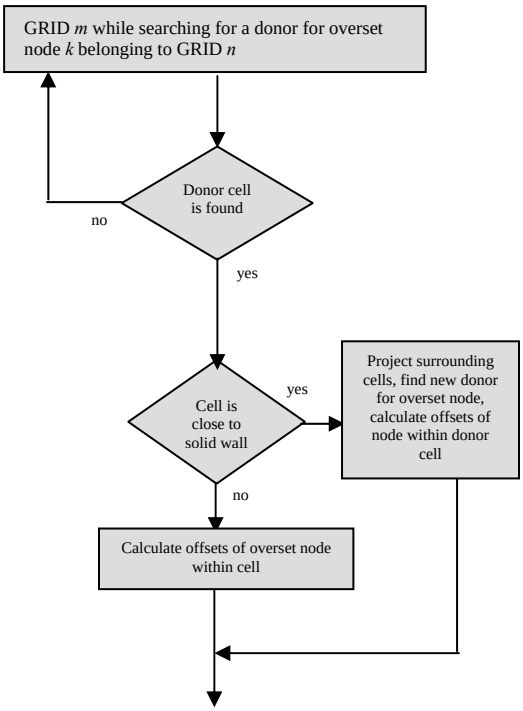

Figure 5. Flow Chart of the Projection Algorithm

The procedure for projecting surrounding cells involves determining the equivalent boundary node (node *w*) in the reference grid (GRID *n* above). Then the boundary cell of the active grid (GRID *m*) is projected in the direction of its normal such that the node w lies on its boundary side as shown in Figure 4. All surrounding cells are also projected as a ratio of their distance from the boundary such that the opposite boundary cell is not projected at all but retains its original coordinates. This approach is also used in PEGASUS.[25]

If the equation of the surface normal of the boundary cell is ($Ax + By + Cz + D = 0$), the projection distance, d of the boundary cell can be calculated as

$$d = Ax_w + By_w + Cz_w + D$$

where (x_w, y_w, z_w) is the coordinate of the candidate boundary node.

For projections along the *k*-axis, for instance, boundary cells and surrounding cells are projected using the equation:

$$x_{new} = x_{\mathbf{old}} + d \cdot A \frac{K_e - k}{K_e - 1}$$

$$y_{new} = y_{\mathbf{old}} + d \cdot B \frac{K_e - k}{K_e - 1}$$

$$z_{new} = z_{\mathbf{old}} + d \cdot C \frac{K_e - k}{K_e - 1}$$

where K_e is the limit of nodes in the *k*-direction and *k* is the index of the current cell in the *k*-direction.

A new search is conducted for a donor cell, in case, the projection has caused the overset node to have shifted to a new donor cell. The offset of the overset node within the identified donor cell is calculated and returned along with the index of the donor cell (as illustrated in Figure 5).

2.3 Interpolating and Donating Solution Values to Overset Nodes

The process of identifying of the donor cell in section 2.2 above yields the value of the corner node of the donor cell as well as the value of the offsets. During the solution process, when boundary conditions are applied, interpolation is done using a high order stencil based on the corner node of the donor cell. Although, this step needs to be performed as part of the solver process, Steps 1 and 2 may be completed as a pre-processing step, except for moving boundary problems.

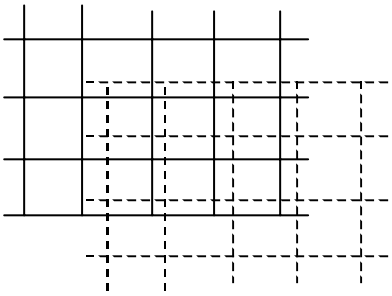

(a) 2D Overlap

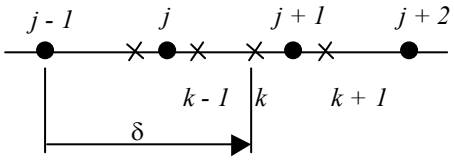

(b) 1-D Overlap

Figure 6. Interpolating stencil for an overset node

Consider a non-coincident overlap of two grids illustrated in Figure 6. The task is to determine the values of solution variables at a nodal point of a receptor grid using the value of known nodal points of a donor grid. The one-dimensional case is shown for simplicity in Figure 6b. For the receptor or overset node, *k*, a third-order interpolation utilizing a central stencil would use the nodes *j-1*, *j*, *j+1*, and *j+2* of the donor grid. The equation for the Lagrange procedure within a unit-spaced grid[26] is

$$\phi = \sum_{k=0}^{m-1} \left(\prod_{\substack{i=0 \\ i \neq k}}^{m-1} (\delta - i) \right) R(k) \phi_k$$

$$R(k) = \frac{-1^{m+k-1}}{(m-k-1)!k!}$$

Here, *m* is the pre-determined order of the interpolant and δ is the distance of the interpolated point from the left-most point of the stencil.

In three-dimensions, a tensor product of piece-wise, high-order interpolation is done using the same Lagrange interpolation procedure in every direction.

2.4 Shock-Capturing Interpolation Procedures

The default choice of interpolating stencil is a central one as described above. For shock-capturing capabilities, the stencil containing *m* nodal points is adapted based on the solution variable *f,* according to the algorithm below:

```
shift = 0
For k = -m/2 + 1, …, m/2
    If ((k + shift) > 0)
            If (|f(I + k + shift - 1)| > ε|f(I + k + shift)|)
                    shift = shift - 1
    Else
            If  (ε|f(I + k + shift + 1)| < |f(I + k + shift)|)
                    shift = shift + 1
    End If
End For
```

In the above algorithm, ε, is a value greater than 1, that is adjusted to fit the magnitude of discontinuity intended to be captured by the scheme.

As an example, consider a third-order interpolation (using 4 points) containing a discontinuity at node *j+2*. The stencil-shifting algorithm will result in an interpolation based on nodes beginning at *j-2* rather than *j-1* as shown in the figure below. Note that, for piece-wise three-dimensional interpolation, the interpolation order may be reduced when interpolating in the secondary directions.

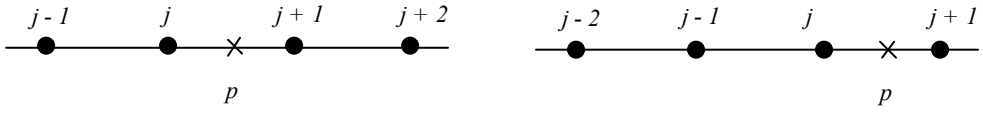

(a) Centered stencil

(b) A stencil used for interpolating $j + ½$ when discontinuity exists at $j + 2$.

Figure 7. A 4-point stencil showing the resulting interpolation stencil adopted for the point p in the presence of a discontinuity at the $(j+2)$th nodal point. A stencil to the right of j+ may also be used, depending of the value of the solution variable.

3. The WENO Procedure

The WENO scheme is a special type of ENO that uses a weighted combination of the trial stencils in the ENO scheme. The latter was developed for solving hyperbolic systems involving discontinuities.[23,24] It can achieve uniformly high-order accuracy with sharp, essentially non-oscillatory shock transitions. The procedure is based on the Godunov approach and the basic principles of upwind schemes, wherein an adaptive stencil (based on difference tables) is used in a locally smoothest region. This strategy provides a strong inhibition towards differencing across discontinuities.

The WENO scheme is applied to the convective terms of the flow equations. For the sake of simplicity, consider the one-dimensional scalar conservation law:

$$\frac{\partial u}{\partial t} + \frac{\partial f(u)}{\partial x} = 0 .$$

The flux term, which is the second term on the left-hand side, can be written as a conserved flux difference

$$\left(\frac{\partial f}{\partial x}\right)_{x=x_j} \approx \frac{1}{\Delta x}(\hat{f}_{j+1/2} - \hat{f}_{j-1/2}) ,$$

where the numerical fluxes on the right hand side approximate $h(x_{j\pm½})$ to a higher order with $h(x)$ defined as

$$f(u(x)) = \frac{1}{\Delta x}\int_{x-\Delta x/2}^{x+\Delta x/2} h(\xi)d\xi .$$

Note that, by Liebnitz rule, we have

$$\frac{\partial f}{\partial x} = \frac{1}{\Delta x}\big(h(x+\Delta x/2) - h(x-\Delta x/2)\big).$$

To approximate $h(x_{j\pm½})$ to a higher order, the primitive function $h(x)$ is used:

$$H(x) = \int_{-\infty}^{\infty} h(\xi)d\xi$$

At $x_{j\pm½}$

$$H(x_{j+1/2}) = \int_{-\infty}^{x_{j+1/2}} h(\xi)d\xi$$

$$= \sum_{k=-\infty}^{j}\int_{x_{j-1/2}}^{x_{j+1/2}} h(\xi)d\xi = \Delta x\sum_{-\infty}^{j} f(u_k) ,$$

so that

$$H\lfloor x_{j-1/2}, x_{j+1/2}\rfloor = \Delta x \cdot f(u_j),$$
$$H\lfloor x_{j-1/2}, x_{j+1/2}, x_{j-3/2}\rfloor = \Delta x \cdot f(u_j, u_{j+1}).$$

The square brackets denote undivided differences. Hence, the $(k + 1)$th order undivided difference of $H(x)$ can be obtained recursively from the kth order undivided difference of $f(u)$. Then the numerical flux can be expressed by a high order interpolation polynomial:

$$f_{j+1/2} = \sum_{k=0}^{md} c(i-j,k)\cdot f[i,k],$$

with i being the left-most point of the stencil used to approximate the flux. $f[i,k]$ is defined by

$f[i,0] = f(u_i)$
$f[i,1] = f[i+1,0] - f[i,0] = f(u_{i+1}) - f(u_i)$
……
$f[i,k] = f[i+1,k-1] - f[i,k-1] = f(u_{i+1}) - f(u_i)$

and $c(s,k)$ by

$$c(s,k) = \frac{1}{(k+1)!}\sum_{l=s}^{s+k}\prod_{\substack{p=s \\ p\neq l}}^{s+k}(-p)\cdot$$

The constant array $c(s,k)$ is computed once and stored.

The stencil adaptation procedure is as shown in section 2.4, except that a weighted combination of the stencil points is used.

4. Validation

4.1.1 Smooth Fields

The procedure for smooth fields was validated using two overset grids with a continuous analytic test function, similar to the procedure in Sherer and Scott:[20]

$$g(x,y) = \frac{0.27x}{x^4 + 9(y^2+9)}\cos\left(\frac{20x}{y+3}\right)\sinh\left(\frac{y}{3}\right)\cdot$$

Interpolated values of the function in one grid are compared with the exact values of the function. The error was computed as the sum of all the errors at each node according to the formula

$$E = \sum\frac{|g-\hat{g}|}{g}$$

where $\hat{g}$ is the value of g obtained from a donor grid and the summation is over the total of all overset nodes. The equation for the mesh used is

$x_{i,j} = x_{min} + i\Delta x$
$y_{i,j} = y_{min} + i\Delta y$
$\Delta x = L_x/(N-1)$
$\Delta y = L_y/(M-1)$
$L_x = x_{max} - x_{min}$
$L_y = y_{max} - y_{min}$
$i \in [1, N]$
$j \in [1, M]$

Four grids were used with the following limits:

Grid 1
$(x_{min}, y_{min}) = (0,0)$, and $(L_x, L_y) = (0.85, 0.60)$.

Grid 2
$(x_{min}, y_{min}) = (0,47)$, and $(L_x, L_y) = (0.85, 1.0)$.

Grid 3
$(x_{min}, y_{min}) = (0.75,0)$, and $(L_x, L_y) = (1.51, 0.60)$.

Grid 4
$(x_{min}, y_{min}) = (0.75,47)$, and $(L_x, L_y) = (1.51, 1.0)$.

The values of N and M were varied for different values of mesh spacing, Δx.

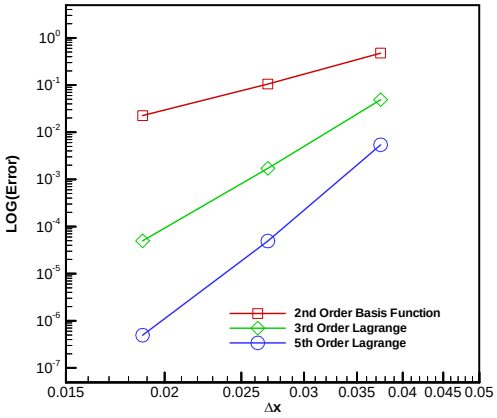

Figure 8. Error analysis of selected interpolation methods for a continuous function

Figure 8 shows the graph of the error for selected interpolation methods. The calculations indicate superior performance of the higher order methods when compared to the second method. For the accuracy and effort required, the fifth-order

Lagrange interpolation scheme performed relatively well compared to the other methods.

4.1.2 Discontinuous Fields

The procedure for discontinuous fields was validated using two overset grids with discontinuous analytical test functions. The mesh used was similar to that for the bow shock problem[23] but contained two overlapping domains. The mesh for each grid contained 121 x 47 x 3 nodal points and was generated with the following equations:

Grid 1

$$x = -\left[R_x - (R_x - 1)\frac{i-1}{N-1}\right]\cos\left[\frac{5\pi}{12}\left(\frac{2(j-1)}{1.77M} - 1\right)\right]$$

$$y = -\left[R_y - (R_y - 1)\frac{i-1}{N-1}\right]\sin\left[\frac{5\pi}{12}\left(\frac{2(j-1)}{1.77M} - 1\right)\right]$$

$$z = k - 1$$

$$R_x = 3.0, R_y = 5.7$$

Grid 2

$$x = -\left[R_x - (R_x - 1)\frac{i-1}{N-1}\right]\cos\left[\frac{5\pi}{12}\left(\frac{2(j-1)}{2M} - 1\right)\right]$$

$$y = -\left[R_y - (R_y - 1)\frac{i-1}{N-1}\right]\sin\left[\frac{5\pi}{12}\left(\frac{2(j-1)}{2M} - 1\right)\right]$$

$$z = k - 1$$

$$R_x = 3.0, R_y = 6.0$$

where

$$(1 \le i \le N), (1 \le j \le M), (1 \le k \le L)$$

and $(N, M, L) = (121, 47, 3)$ for both grids.

The discontinuous function is

$$\begin{cases} g = 0.8r^4 + 0.4r^2 \sin\left(\dfrac{2x^5}{y + 3r^3}\right) & r > 2 \\ g = 0.1r^4 + 0.01r^2 \sin\left(\dfrac{2x^5}{y^2 + 4r}\right) & r \le 2 \end{cases}.$$

Two cases were tested for each interpolation function. The first case uses the values of R_x and R_y indicated above while the second case used half the values of R_x and R_y for both grids. The results are shown in figure 9. The same formula as that used for smooth fields for measuring the error at each overset grid point was used. The high order methods performed better than the low order method. However, the shock-capturing method which selects interpolation stencils away from discontinuities performed significantly better than the interpolation method of the same order.

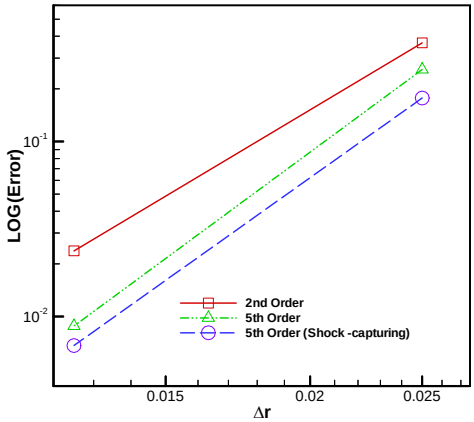

Figure 9. Error analysis of selected interpolation methods for a discontinuous function. Δr is the mesh size in the radial direction.

4.1.3 Investigation of Flux Conservation Properties of Smooth Fields

The flux preservation properties of the overset procedure were evaluated to ensure that fluxes of the solution variables were preserved across an overlap region. The test was conducted across two overlapping grids in a 2D calculation. The Navier-Stokes equations are solved in general curvilinear coordinates employing the compact scheme with compact filters. The two grids are shown in the figure 10.

The fluxes are defined as

$$F = \begin{bmatrix} \rho u^2 + p \\ \rho uv \end{bmatrix}$$

and

$$G = \begin{bmatrix} \rho uv \\ \rho v^2 + p \end{bmatrix}.$$

The values of the fluxes were computed to the one side of the overlap of a donor grid and to the other side of the overlap of the recipient grid using the second order and the fifth order Lagrange interpolation methods. The results are illustrated in figure 11 and shows that the fifth order procedure preserved the fluxes across the overlap. The second

order procedure shows visible differences across the overlap.

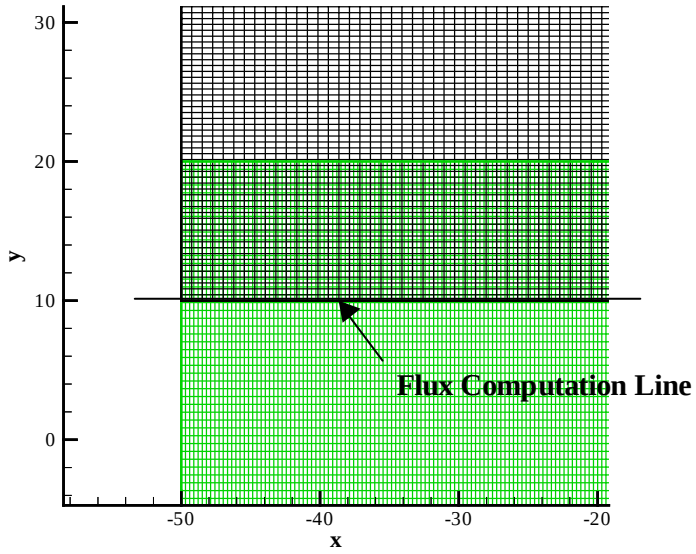

Figure 10. Grids used in the test of flux conservation properties of the overset scheme

4.2 Demonstration of High Order

The validation of the overset procedure for smooth and discontinuous fields discussed in 5.1 show that the high-order procedure conveys solution variables more accurately across an overlap region. This was also confirmed by the flux preservation investigation performed in 5.2. Consequently, overlapped domains using high-order interpolation procedures to transfer results will provide more accurate boundary conditions for a CFD calculation, particularly for a high-order solver.

5. Results

Three problems used to illustrate the procedure described in this paper: subsonic flow past a circular cylinder and a sphere, and supersonic flow over a circular cylinder. These are discussed in turn below.

5.1 Flow Past a Circular Cylinder

The flow past a circular cylinder was calculated using five overlapping grids at Ma = 0.1, Re = 100 similar to the validation problem in Sherer and Scott.[20] The problem was solved in 2D with fifth-order compact scheme for spatial differencing and fourth order Runge-Kutta for time integration. The central grid enclosed the cylinder surface and was constructed such that the mesh was densely graded at the wake region. The grid block overlapping the central grid was also graded at the center. The mesh of the entire assembly is shown in figure 12a. There are 121 x 60 nodes in each block. The fifth order interpolation scheme was used. Each block was assigned to a processor of a parallel machine. The results were compared to those from a single grid containing 197 x 144 nodal points, with a radius 25 times the diameter of the cylinder.

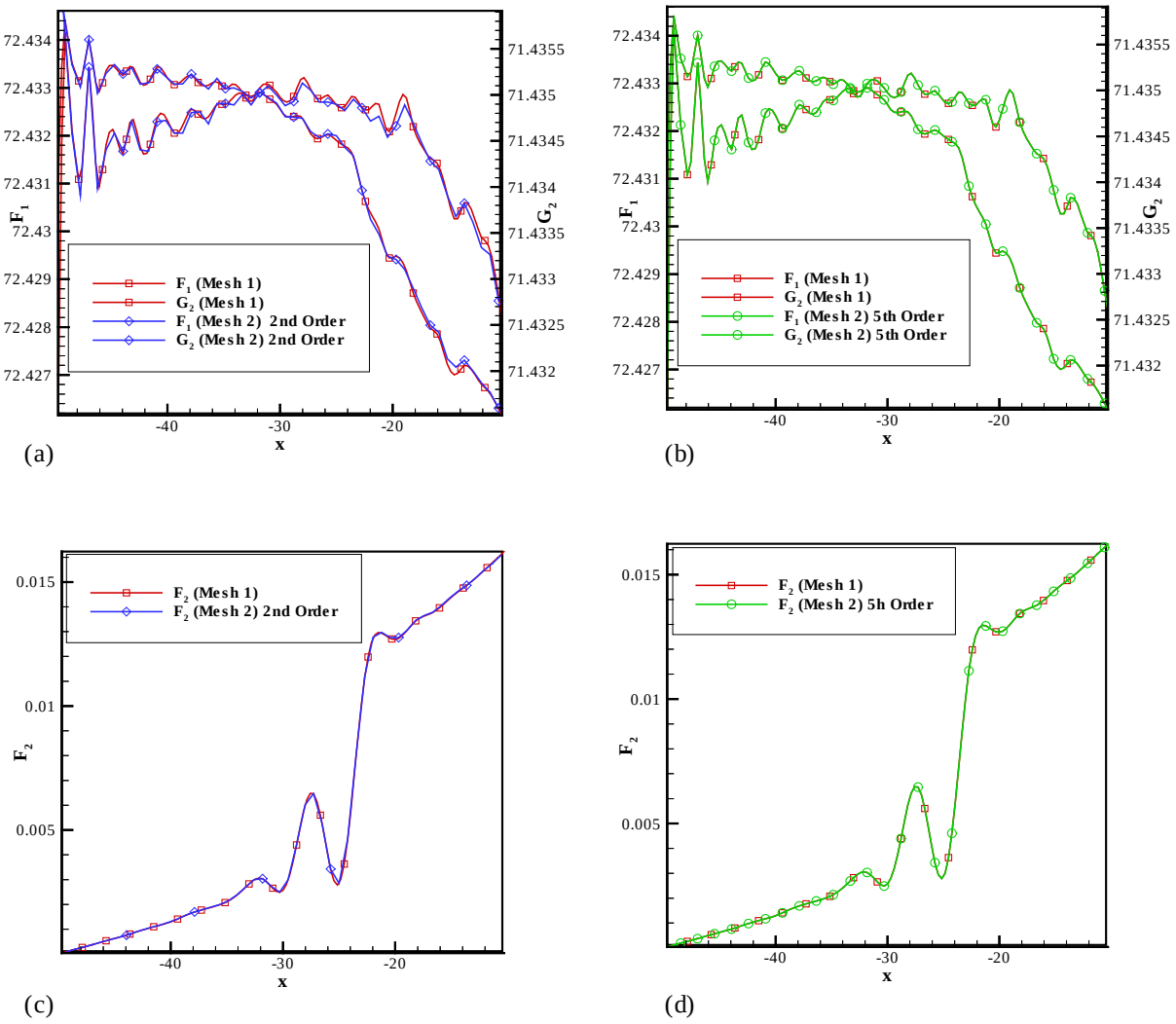

Figure 11. Flux conservation properties of the overset procedure

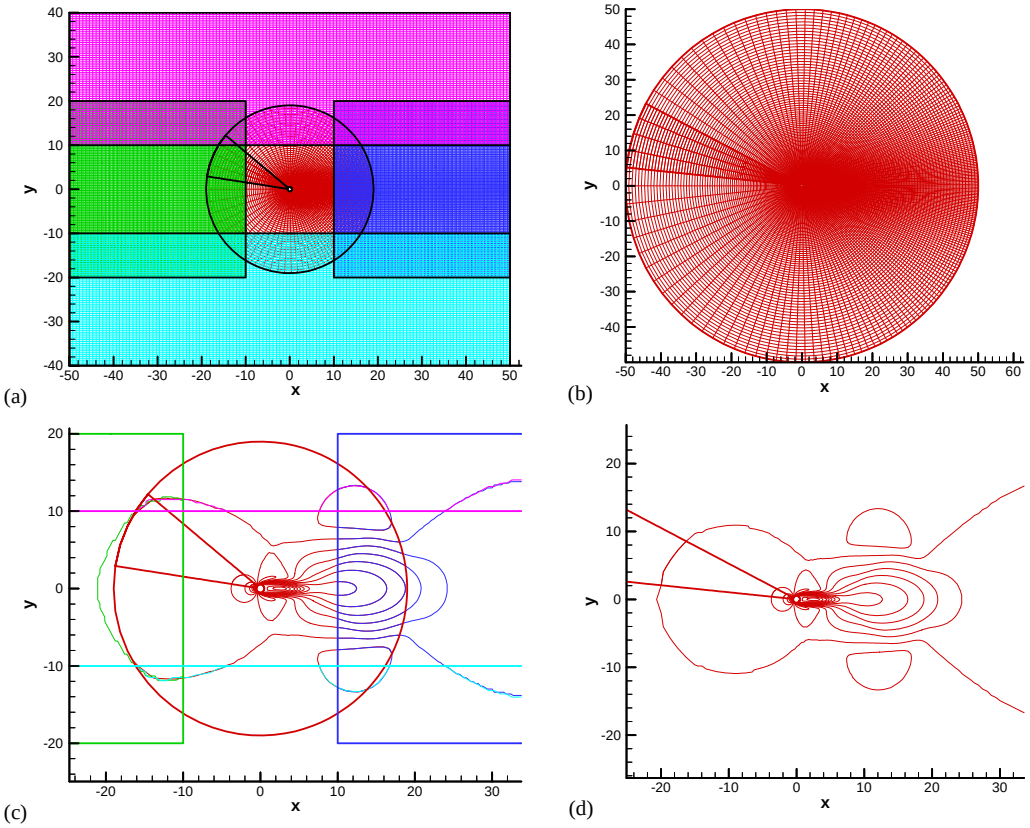

Figure 12. Mesh and results for flow over a circular. (a) Overset grid, (b) single domain grid, (c) Mach number contour (overset grid), (d) Mach number contour (single domain grid).

The differences in the two solutions were compared and are shown in Figure 12 for pressure. The largest difference (error) occurred in the pressure solution, with a magnitude of approximately 7.746 x 10^{-5}%. Figure 13 shows the Von Karman vortex street at the wake of the cylinder. The maximum value of the coefficient of drag was calculated as 1.311, which compares well with the value of 1.310 reported by Visbal and Gaitonde[27] using a similar solver as the present one.

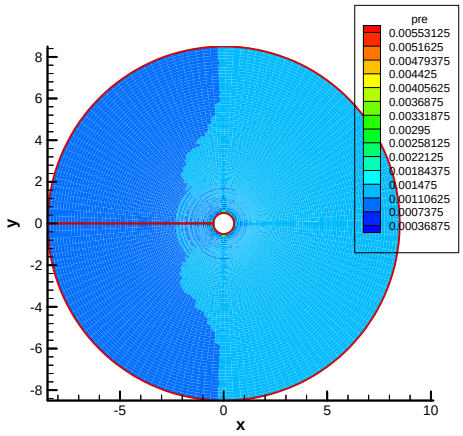

Figure 13. Difference contours for pressure derived from calculations in the overlapped domain and the single domain

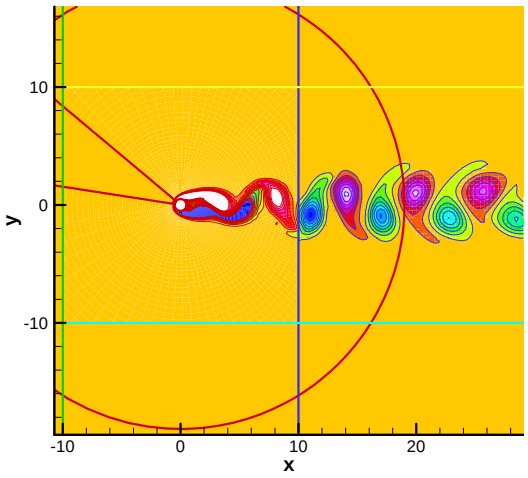

Figure 14. Convecting vortices from the wake of the circular cylinder flowing across overset grids

5.2 3D Flow Past a Sphere

The overset procedure was also validated for flow over a 3D sphere at Re = 100, Ma = 0.1. The overlapped domain consisted of 6 blocks, each containing a segment of the sphere surface as shown in Figure 15. Each block contained 25 x 25 x 25 nodal points and was assigned to a separate processor in a parallel machine. Spatial and temporal differencing were similar to the case discussed in section 5.1. Since each block contains a segment of the sphere surface, the projection features available within the overset scheme was needed to ensure accurate solution close to the surface of the sphere. Fifth order interpolation methods were used in order to match the order of the spatial differencing scheme.

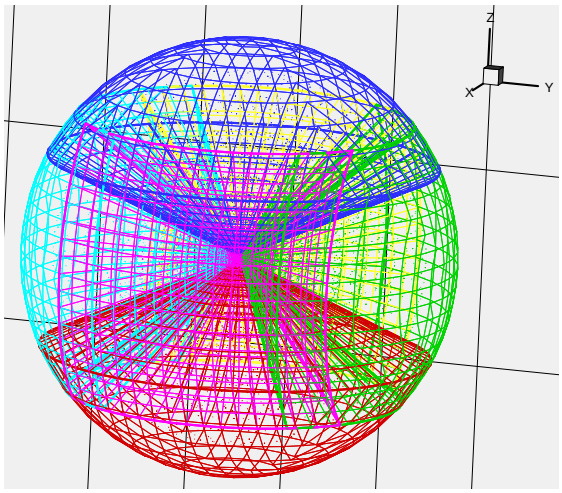

Figure 15. Six overset grids for flow over a sphere.

Figure 16 shows the streamlines downstream of the sphere. Qualitative agreement with the results in Patel & Johnson[28] is evident. Also, the average value of drag was 1.235 compared to the value of 1.20±15% reported in the literature[29].

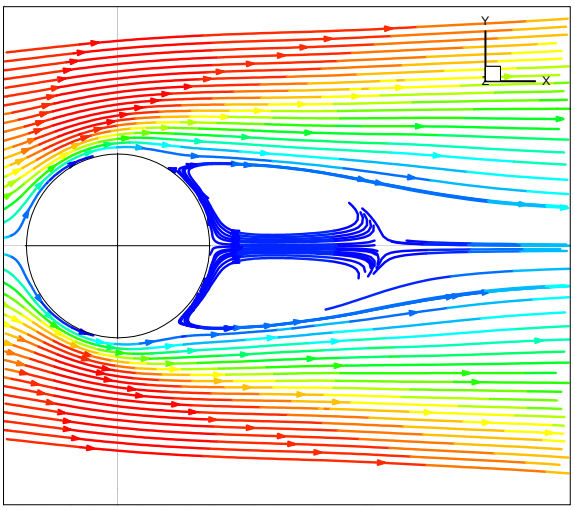

Figure 16. Streamlines of flow past a sphere

4.6 Bow Shock Problem

The overset procedure described in this paper was used to calculate the bow-shock[23] problem. The problem involved flow over the nose of a circular cylinder at Ma = 2.15 and Re = 3.9 x 10^6. The problem was solved in 3D with two overlapping domains each 121 x 47 x 3. The WENO procedure was used for this calculation with the beam

warming procedure for time integration. Two meshes were used to solve the problem. The first contains an overlap but with all nodes coincident (usual multi-block problem). The second mesh contains two overset grids. The nodes of the overlapping domains are generally non-coincident. Other than the overlap, both domains are proportionally similar. The grid generation equations for the non-coincident overset grids were previously presented in section 4.1. The overlap mesh used for the problem is shown in Figure 17.

Three interpolation methods were used for calculating values for the overset nodes: (a) the method described in this paper for selecting shock-capturing interpolation stencils, (b) fifth-order central interpolation stencil, (c) second order central interpolation stencil. The solutions obtained using the coincident overset grids represents the fourth calculation. This is used as the reference calculation for the non-coincident overset calculations. All calculations are steady state. Single domain results are used to initialize the overset calculations.

Figures 18 through 20 shows the contour plot for all four calculations for pressure, density and u-velocity respectively. The figures show that all calculations preserve the shock profile for the problem. This is due to the fact that the order of the solver is the same for all the four calculations and the approximation at the boundary of the overlap appears to have little effect on the solution far away from the boundary. However, for the low-order calculation, some differences can be observed far away from the overset boundary, particularly for the density and velocity calculations.

Figures 21 through 23 show the results along selected radial lines - four, seven, and fourteen azimuthal nodes from the overset boundary. The results again confirm that, except for the low-order procedure, all interpolation methods compared well with the reference and the errors become smaller as the distance from the overset boundary increases. A close up on the results in the vicinity of the shock shows superior performance for the shock-capturing interpolation method presented in this paper (Figure 24).

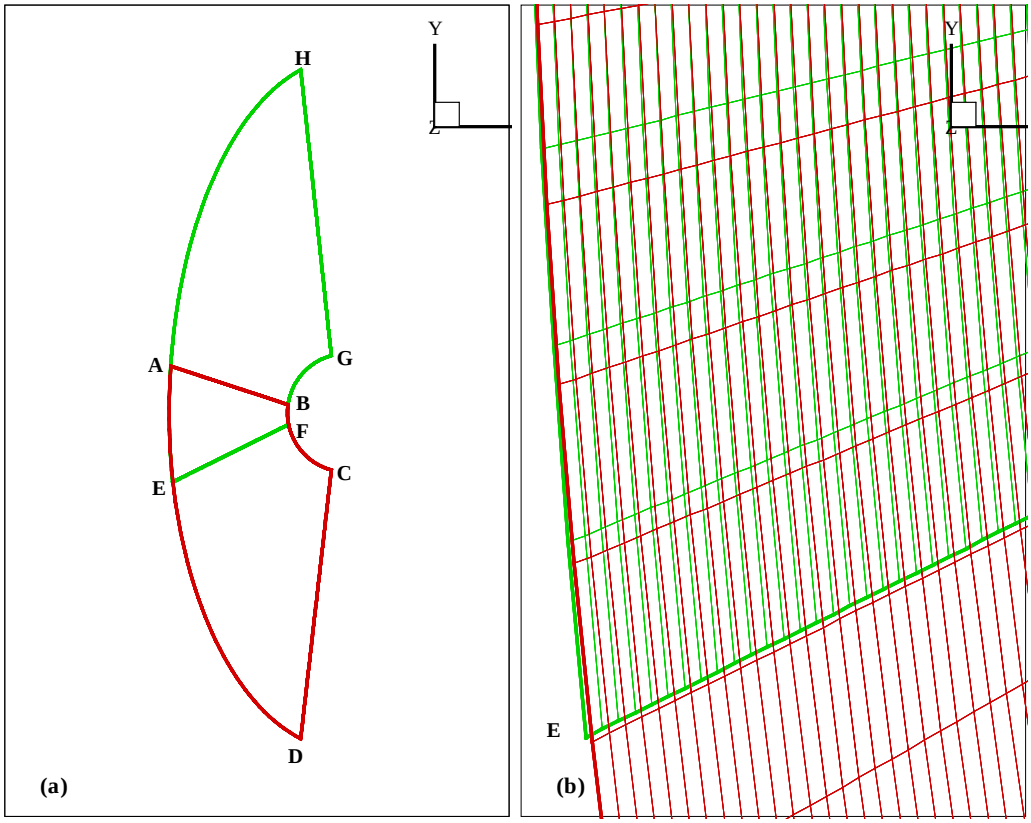

Figure 17. Two overset grids and a close up on the vicinity of the boundary AE and EF (Block 1: ABCDA, Block 2: EFGHE)

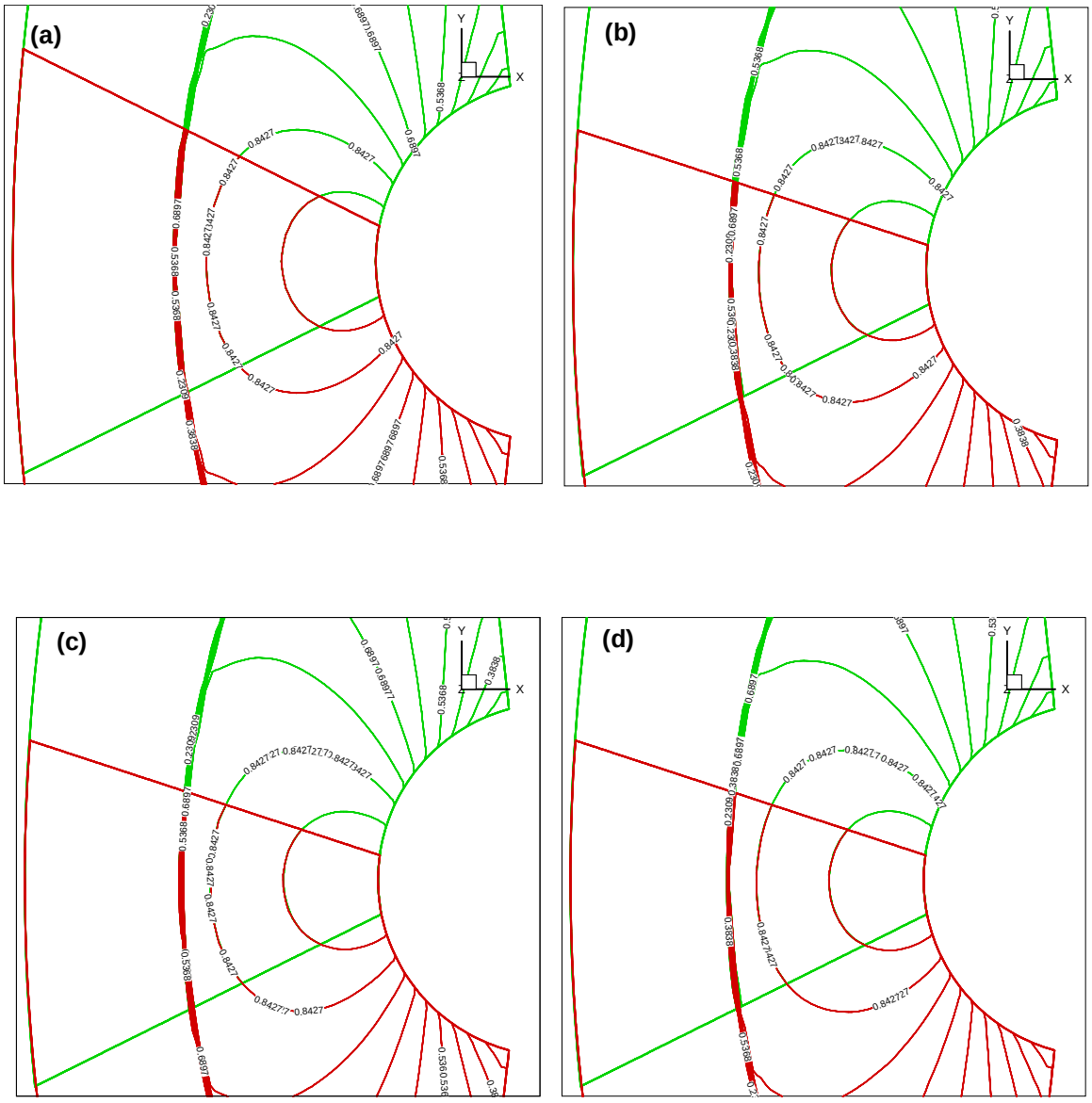

Figure 18. Pressure contour (a) Overlap, with coincident nodes, (b) Non-coincident overlap, 5th order, shock-capturing interpolation, (c) Non-coincident overlap, 5th order central interpolation stencil, (d) Non-coincident overlap, 2nd order central interpolation stencil

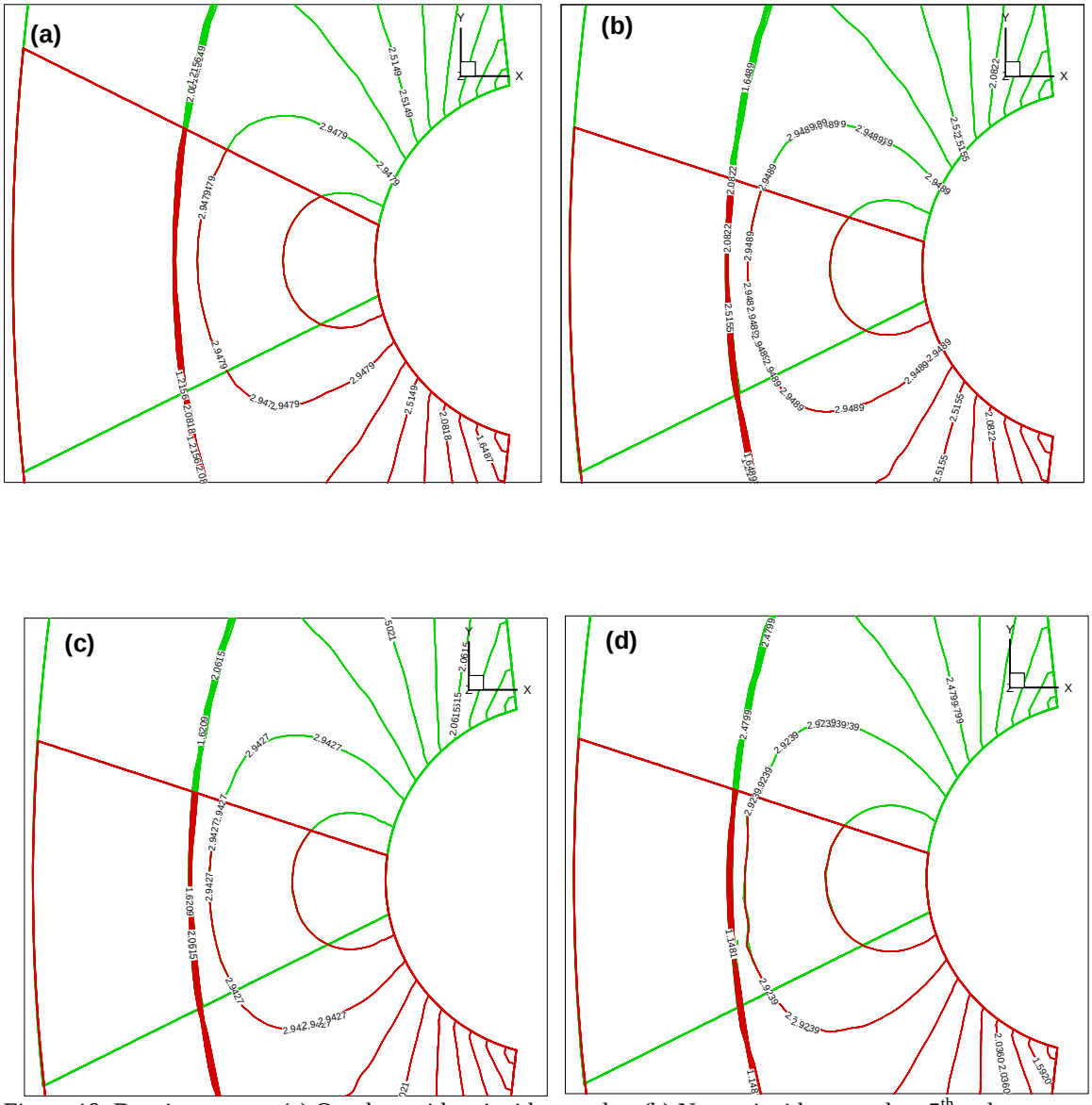

Figure 19. Density contour (a) Overlap, with coincident nodes, (b) Non-coincident overlap, 5th order, shock-capturing interpolation, (c) Non-coincident overlap, 5th order central interpolation stencil, (d) Non-coincident overlap, 2nd order central interpolation stencil

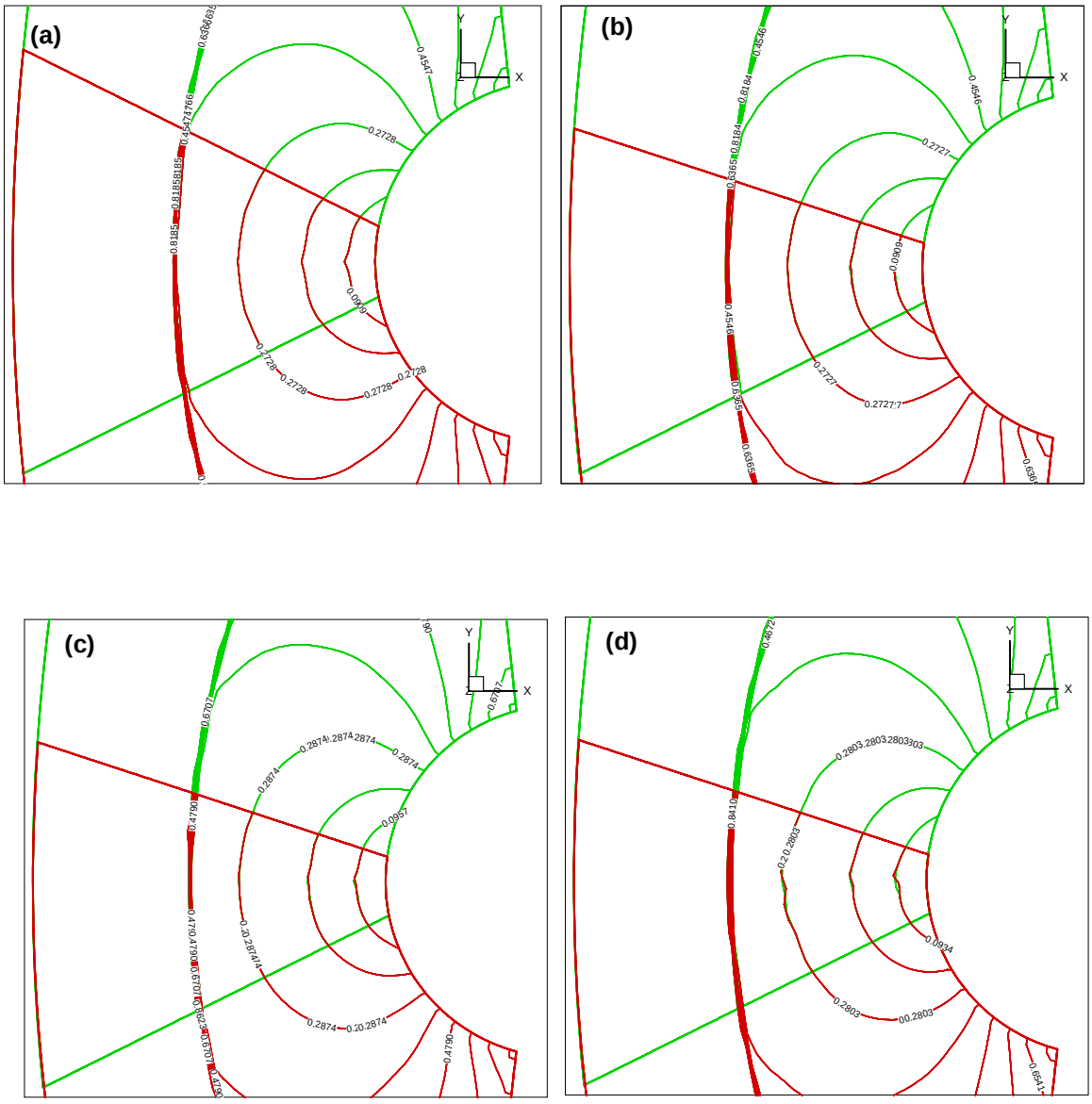

Figure 20. *u*-velocity contour (a) Overlap, with coincident nodes, (b) Non-coincident overlap, 5th order, shock-capturing interpolation, (c) Non-coincident overlap, 5th order central interpolation stencil, (d) Non-coincident overlap, 2nd order central interpolation stencil

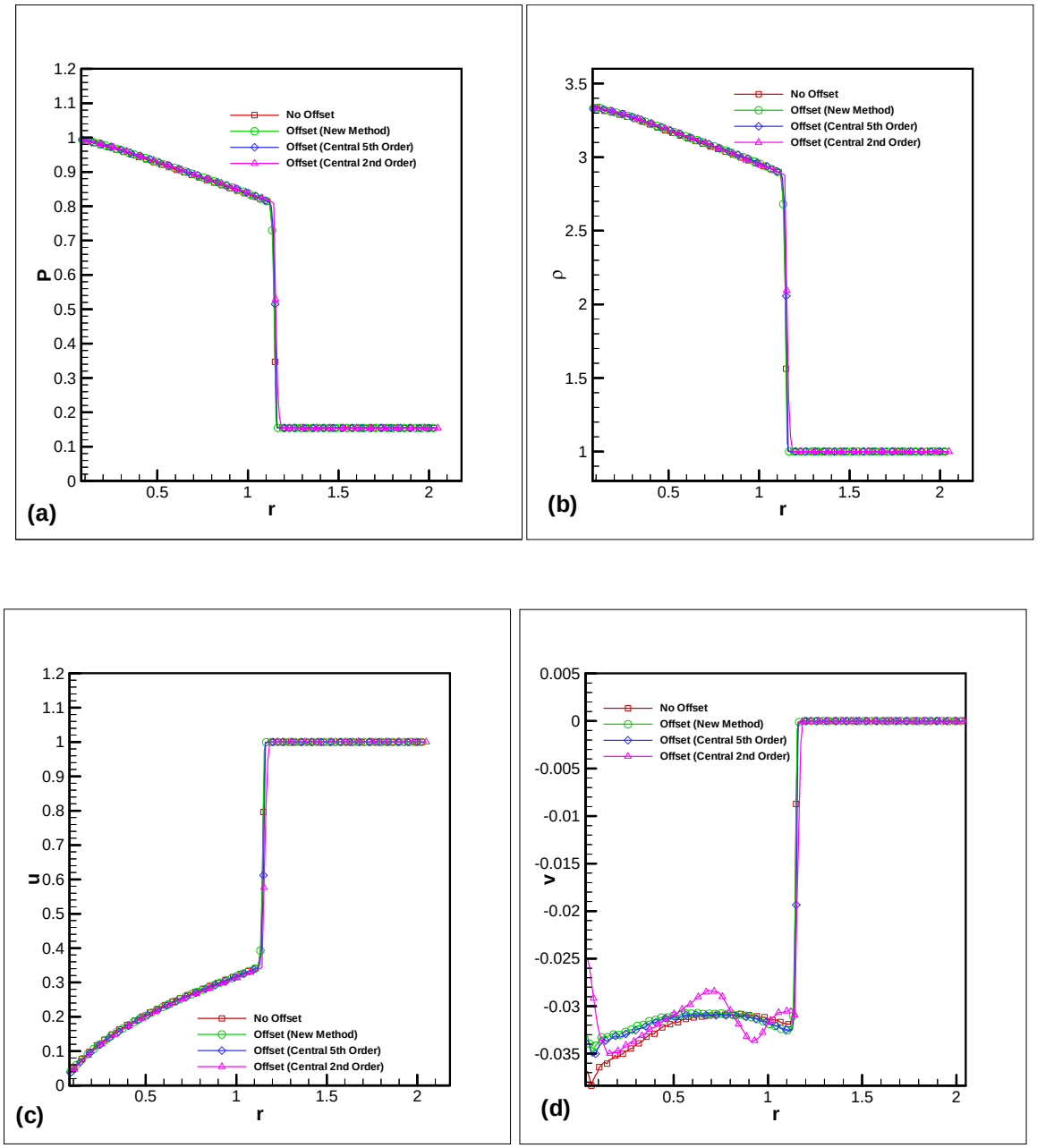

Figure 21. Results extracted along a line that is four nodes removed from the overlap (a) Pressure, (b) Density, (c) *u*-velocity, (d) *v*-velocity. *r* is the distance from the surface of the cylinder.

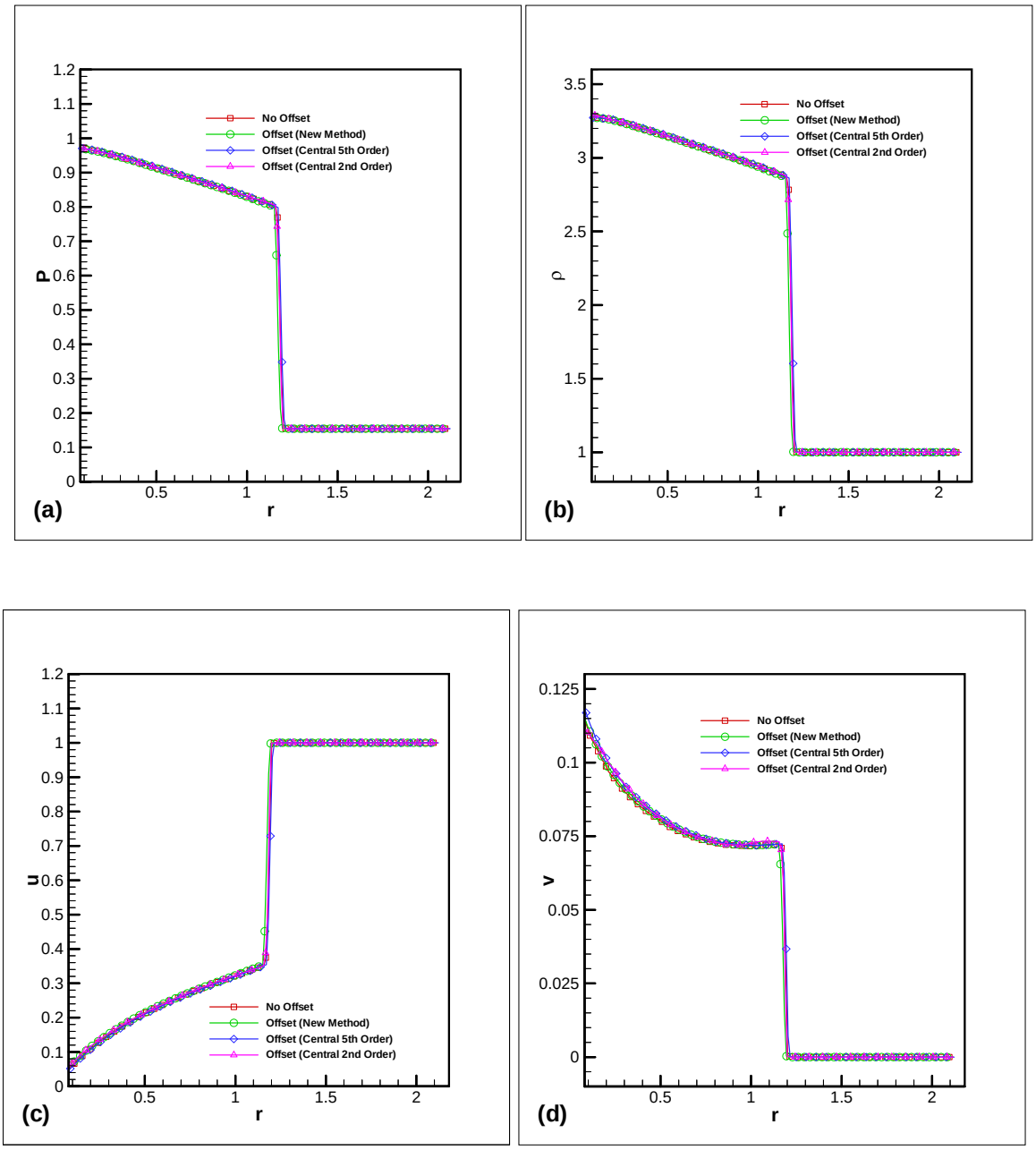

Figure 22. Results extracted along a line that is seven nodes removed from the overlap (a) Pressure, (b) Density, (c) *u*-velocity, (d) *v*-velocity. *r* is the distance from the surface of the cylinder.

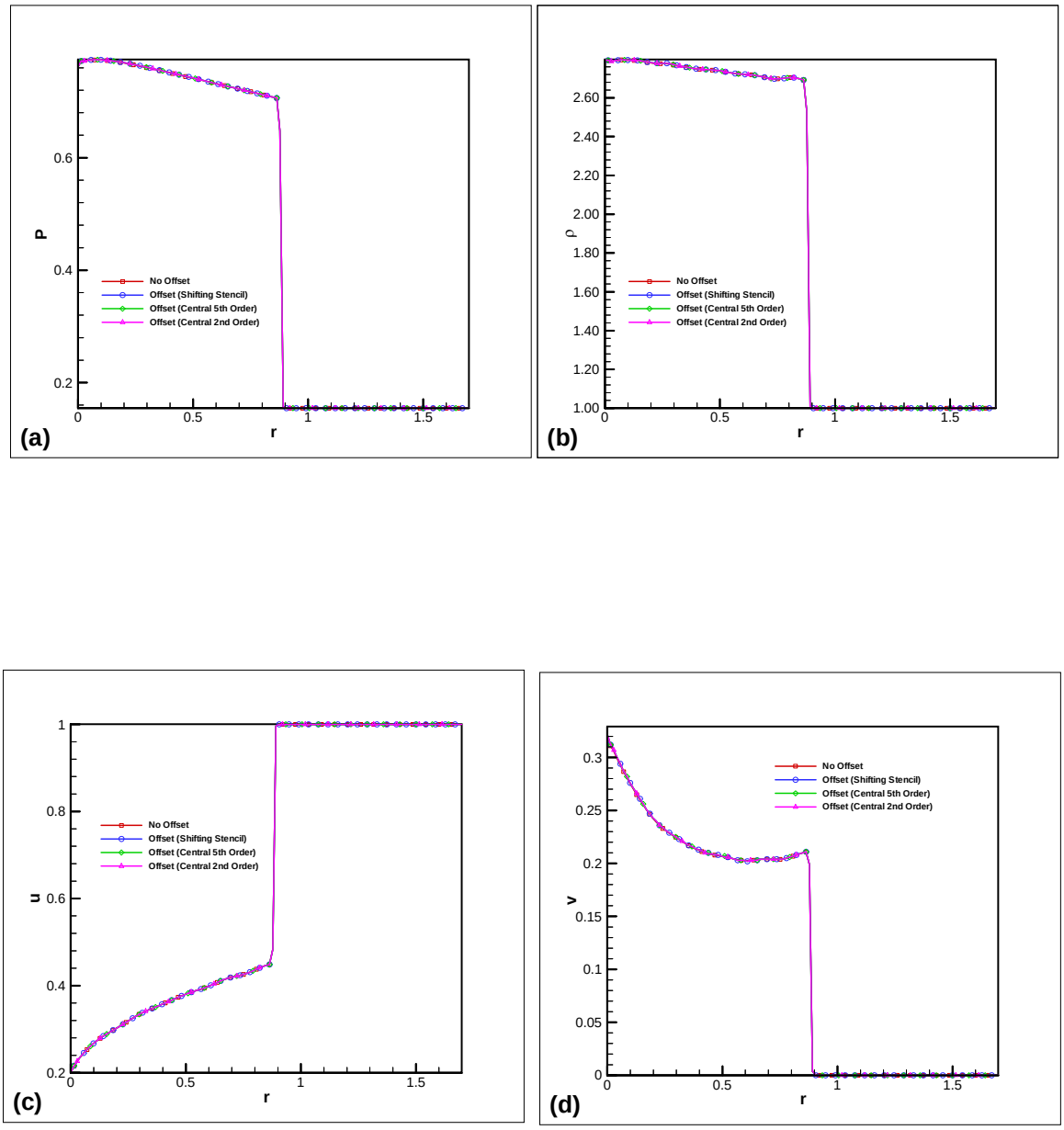

Figure 23. Results extracted along a line that is fourteen nodes removed from the overlap (a) Pressure, (b) Density, (c) *u*-velocity, (d) *v*-velocity. *r* is the distance from the surface of the cylinder.

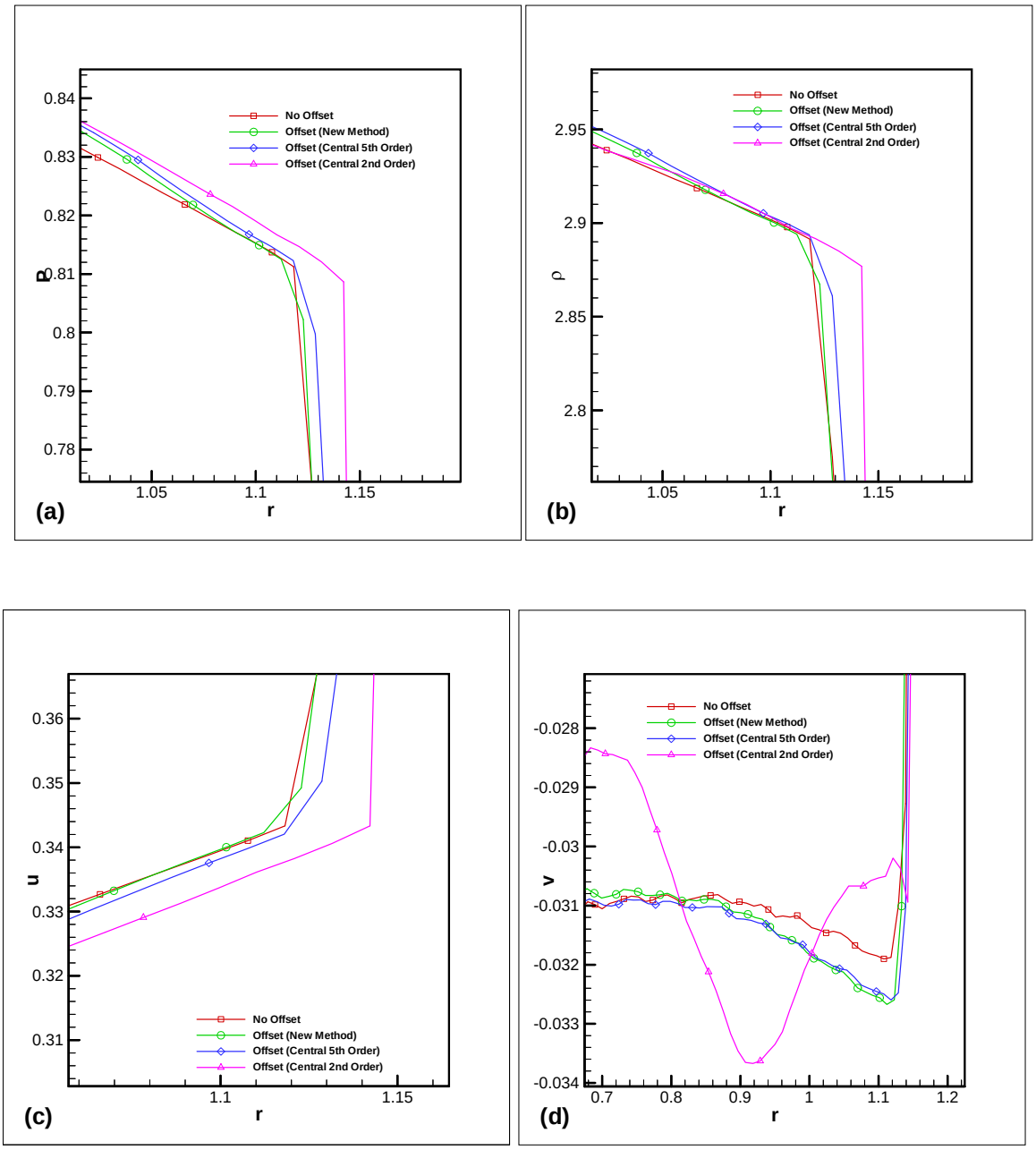

Figure 24. Results near the shock along a line that is four nodes removed from the overlap (a) Pressure, (b) Density, (c) *u*-velocity, (d) *v*-velocity. *r* is the distance from the surface of the cylinder.

5. Concluding Remarks

In this paper, we report on a high-order overset procedure for smooth flow fields and flow fields with discontinuities. Validation of the procedure is discussed, as is its flux conservation. The procedure is illustrated with the calculation of flow over a cylinder and sphere. Calculations of the bow shock over a circular cylinder were also carried out. Results show the high order interpolation procedure to be the most accurate in providing interpolated data at the overlap region. For discontinuous fields, the newly introduced shock-capturing interpolation procedure shows significant improvement in the vicinity of the discontinuities.

References

[1]Lele, S.K., "Compact Finite Difference Schemes with Spectral-like Resolution," Journal of computational Physics, Vol.103, 1992, pp16-42.

[2]Visbal, M.R. and Gaitonde, D.V., "High-Order-Accurate Methods for Complex Unsteady Subsonic Flows," AIAA Journal, Vol. 37, No. 10, 1999, pp. 1231-1239.

[3]Rizzetta, D., Visbal, M., and Gaitonde, D., "Direct Simulation and Large-Eddy Simulation of Supersonic Flows by a High-Order Method," AIAA Paper 00-2408, Fluids 2000, Denver, CO, June 2000.

[4]Visbal, M.R., and Gaitonde, D.V., and Gogineni, S.P., "Direct Numerical Simulation of a Forced Transitional Plane Wall jet," AIAA Paper 98-2643, 29h AIAA Fluid Dynamics Conference, Albuquerque, NM, June 1998.

[5]Ladeinde, F., Cai, X., Visbal, M. R., and Gaitonde D.V., "Parallel Computation of Complex Aeroacoustic Systems," AIAA Paper 01-1118, 39th AIAA Aerospace Sciences Meeting, Reno, NV, January 2001.

[6]Freund, J., Lele, S., and Moin, P., "Direct Simulation of a Mach 1.92 Jet and its Sound Effect," AIAA Paper 98-2291, 4th AIAA/CEAS Aeroacoustics Conference, Toulouse, France, June 1998.

[7]Gaitonde D.V., Shang, J., and Young, J., "Practical Aspects of High-Order Accurate Finite-Volume Schemes for Electromagnetics," AIAA Paper 97-0363, AIAA 35th Aerospace Sciences Meeting, Reno, NV, January 1997.

[8]Gaitonde D.V., and Shang, J., "High-Order Finite –Volume Schemes in Wave Propagation Phenomena," AIAA Paper 96-2335, 27th AIAA Plasmadynamics and Lasers Conference, New Orleans, LA June 1996.

[9]Shang, J., "High-Order Compact Difference Schemes for Time- Dependent Maxwell Equations," Journal of Computational Physics, vol. 153, 1999, pp.312-333.

[10]Steger, J. L., Dougherty, F.C., and Benek, J.A., " A Chimera Grid Scheme," Advances in Grid Generation, edited by K. Ghia and U. Ghia, ASME-FED-Vol5, the American Society Of Mechanical Engineers, 1983, pp.59-69.

[11]Benek, J., Steger, J., and Dougherty, f., "A Flexible Grid Embedding Technique with Application to the Euler Equation," AIAA Paper 83-1944, 1983.

[12]Benek, J., Buning, P., and Steger, J., "A 3-D Chimera Grid Embedding Technique," AIAA Paper 85-1523, 1985.

[13]Belk, D.M., " The Role of Overset Grids in the Development of the General Purpose CFD Code," Surface modeling, Grid Generation, and Related Issues in Computational Fluid Dynamics (CFD) Solutions, NASA CP-3291, 1995, pp. 193-204.

[14]Rogers S.E., Roth, K., Nash, S.M., Baker, D.M., Slotnick J.P., Whitlock M., Cao H.V. "Advances In Overset CFD Processes Applied to Subsonic High-Lift Aircraft.", AIAA Paper 2000-4216, AIAA Applied Aerodynamics Conference, 2000, Denver Co.

[15]Snyder, R.D. and Scott, J.N., "An Overset Grid Solver With Method Coupling and Feature Tracking," AIAA Paper 99-3290, 1999.

[16]Josyula, E and Gordnier, R.E., " Computational Simulation of the F-22 Aircraft," AIAA Paper 98-0526, 36th Aerospace Sciences Meeting, Reno, NV, January 1998.

[17]Yin, J and Delfs, J., " Sound Generation from Gust- Airfoil Interaction Using CAA-Chimera Method," AIAA Paper 01-2136, 7th AIAA/CEAS

Aeroacoustics Conference Maastricht Netherlands, May 2001.

[18]Delfs, J.W., " An Overlap Grid Technique for High Resolution CAA Schemes for complex Geometries," AIAA paper 01-2199, 7th AIAA/ CEAS Aeroacoustics Conference Maastricht Netherlands, May 2001.

[19]Lee, Y. and Baeder, J.D., "High-Order Overset Method for Blade Vortex Interaction," AIAA Paper 02-0559, AIAA 40th Aerospace Sciences Meeting Reno, NV, January 2002.

[20]Sherer, S.E & Scott, J.N., 2002. Development and Validation of a High Order Overset Grid Flow Solver". AIAA Paper 2002-2733.

[21]Liu, W., 1999, "Numerical Studies of Compressible Turbulence" M.S. Dissertation, SUNY Stony Brook, 1996.

[22]Ladeinde, F., Liu, W., O'Brien, E. E., 1998. " Turbulence in Compressible Mixing Layers", Journal of Fluid Engineering , Vol 120, pp 48-53.

[23]Jiang, G. -S. and Shu, C. -W. "Efficient Implementation of Weighted ENO Schemes", J. Comput. Phys., Vol 126, 202, 1996.

[24]Shu, C.W., 1997. " Essentially Non-Oscillatory and Weighted Essentially Non-Oscillatory Scheme for Hyperbolic Conservation Laws", ICASE Report 97-65.

[25]Rogers, S., Suhs, N. and Dietz, W., "PEGSUS 5.0 User's Manual" Technical Report AEDC-TR-91-8, Arnold Engineering Development Center, November 1991.

[26]Wylie, C.R. and Barrett, L.C., 1982. Advanced Engineering Mathematics, McGraw-Hill Book Company, 5th ed .

[27]Visbal, M.R., and Gaitonde, D.V., "High-Order Accurate Methods for Unsteady Vortical Flows on Curvilinear Meshes," AIAA Paper 98-2643, 29h AIAA Fluid Dynamics Conference, Albuquerque, NM, June 1998.

[28]Patel, V. C. and Johnson, T. A., "Low Reynolds Number Flow Past a Sphere", IIHR Hydroscience and Engineering, The University of Iowa. 2002.